Real-Time Geolocation with a Satellite Formation

Noam Leiter

Graduate Student, Faculty of Aerospace Engineering
Technion - Israel Institute of Technology
Haifa 32000, Israel; (077) 887-1834
noaml@technion.ac.il

Advisor: Pini Gurfil

Associate Professor, Faculty of Aerospace Engineering
Technion - Israel Institute of Technology

Abstract

Space-borne geolocation with a small satellite formation could provide accurate tracking of a Mars rover, a redundant navigation system in a jammed GNNS environment, or a cost-effective system for autonomously locating distress signals. In this study we demonstrate how a cluster of two or three Low Earth Orbit (LEO) satellites performing sequential time difference of arrival measurements could accurately determine the position of a terrestrial source emitting electromagnetic pulses. Whereas TDOA geolocation algorithms have been presented before, this study provides a theoretical basis for achieving optimal positioning performance, while solving for the initial position ambiguity through recursive filtering techniques.

1 Introduction

Time Difference of Arrival (TDOA) positioning, also known as a hyperbolic fix, is part of a larger group of passive positioning methods. Such methods have numerous applications ranging from indoor robot navigation systems, through underwater acoustic positioning, to the Deep Space Network for tracking interplanetary spacecraft.

Various techniques have been developed for geolocating a single source using several receivers. Foy [1] introduced the Iterative Least Squares (ILS) method that was followed by several closed-form solutions proposed by Friedlander [2], Smith and Abel [3] and others. Modern methods, such as genetic algorithms [4] were developed as well. In order to solve for the three unknown emitter coordinates, all methods must use a minimum of three non-trivial TDOA measurements. In geolocation problems, the emitter is located on the geoid and the added constraint allows to solve for the emitter position with two TDOA measurements. Ho and Chan [5] presented an analytic solution with two TDOA measurements obtained by a three satellite formation, with a possible ambiguity of several solutions. We present an augmented iterative method with two TDOA measurements obtained by a two satellite formation.

When several pulses, emitted from the same source, are available, a minimum of two receivers, moving relative to the source, could produce a sequence of TDOA measurements. Various positioning techniques could then be applied, such as an Extended Kalman Filter (EKF) [6], Unscented Kalman Filter (UKF) [7, 8] and Gaussian Measurement Mixture (GMM) [9]. All methods must address the nonlinearity of TDOA measurements and the possible ambiguity in the initial estimate which is critical for the convergence of the estimator. We present a sequential method for solving the initial ambiguity and examine the performance compared to the positioning accuracy limits.

2 System Model

2.1 Beacon Model

The beacon is assumed to be static in the Earth-Centered Earth-Fixed (ECEF) frame $\mathscr{F}$:

$$[\dot{\mathbf{s}_0}]_{\mathscr{F}} = \mathbf{0} \tag{1}$$

Relative to an Earth-Centered Inertial (ECI) frame the beacon dynamics are:

$$\dot{\mathbf{s}}_0 = [\boldsymbol{\Omega}_{\oplus}\times]\,\mathbf{s}_0 \tag{2}$$

where $\boldsymbol{\Omega}_{\oplus}$ is Earth's spin vector,

2.2 Satellite Model

The formation satellites positions, $\{\mathbf{s}_i\}_{i=1}^{N}$, are estimated in the on-board navigation computers. For the geolocation algorithm, the navigation errors are assumed to be stationary and uncorrelated and modeled as Gaussian white noise signals:

$$\tilde{\mathbf{s}}_i = \mathbf{s}_i + \delta\mathbf{s}_i \tag{3}$$

$$\delta\mathbf{s}_i \sim \mathcal{N}(\mathbf{0}, R_s) \tag{4}$$

$$E\left[\delta\mathbf{s}_i\delta\mathbf{s}_j^T\right] = R_s \cdot \delta_{ij} \tag{5}$$

where δ_{ij} is the Kronecker delta:

$$\delta_{ij} = \begin{cases} 1 & i = j \\ 0 & i \neq j \end{cases} \tag{6}$$

It is assumed that the covariance of the true navigation error, $\delta\mathbf{s}_i^*(t)$, is bounded such that:

$$\mathrm{cov}\left[\delta\mathbf{s}_i^*(t)\right] \preceq R_s. \tag{7}$$

A difference vector is defined for each pair of satellites in the cluster,

$$\mathbf{s}_{ji} \triangleq \mathbf{s}_j - \mathbf{s}_i \tag{8}$$

and a line of sight (LOS) vector to the beacon is defined for each of the satellites:

$$\mathbf{s}_{i0} \triangleq \mathbf{s}_i - \mathbf{s}_0 \tag{9}$$

2.3 TDOA Measurement Model

In this study each of the satellites performs a Time-of-Arrival (TOA) measurement $\tilde{t}_i$ and the TDOAs are obtained from the differences. If the TDOAs are obtained with some cross-correlation scheme, a different measurement model should be used. The geolocation algorithm TOA model considered hereafter is:

$$\tilde{t}_i = \frac{1}{c}\sqrt{\mathbf{s}_{i0}^T\mathbf{s}_{i0}} + t_0 + v_i \tag{10}$$

where c is the speed of light and t_0 is the (unknown) time of emission. v_i is the measurement error, a combination of the on-board clock bias $b_i(t_i)$ sampled at the time of arrival t_i and the pulse detection error ε_i:

$$v_i(t_i) = b_i(t_i) + \varepsilon_i \tag{11}$$

For the geolocation algorithm, the on-board clock bias and the pulse detection error are assumed to be zero mean i.i.d Gaussian processes:

$$b_i(t_i) \sim \mathcal{N}\left(0, \sigma_b^2\right) \tag{12}$$

$$\varepsilon_i \sim \mathcal{N}\left(0, \sigma_\varepsilon^2\right) \tag{13}$$

therefore, the TOA measurement error, v_i, is modeled in the geolocation algorithm as white Gaussian noise:

$$v_i \sim \mathcal{N}\left(0, \sigma_t^2\right) \tag{14}$$

where $\sigma_t^2 = \sigma_\epsilon^2 + \sigma_b^2$. It is assumed that the variance of the true clock bias, $b_i^*(t)$, is bounded do to synchronization with GNNS time updates, e.g, GPS pps signal, such that:

$$\mathrm{var}\left[b_i^*(t)\right] \leq \sigma_b^2 \tag{15}$$

2.3.1 Incorporating Navigation Estimates

We consider a system where the navigation filter and the geolocation algorithm are separated, i.e., the navigation estimates enter the geolocation algorithm as an input and not as part of the state. This model induces an additional measurement error as seen in the expansion of $\tilde{t}_i$ to first order in $\delta\mathbf{s}_i$ assuming $\|\delta\mathbf{s}_i\| \ll \|\mathbf{s}_{i0}\|$:

$$\tilde{t}_i \approx \frac{1}{c}\sqrt{\tilde{\mathbf{s}}_{i0}^T\tilde{\mathbf{s}}_{i0}} + t_0 + \mathbf{h}_i^T\delta\mathbf{s}_i + v_i \tag{16}$$

where $\tilde{\mathbf{s}}_{i0} = \tilde{\mathbf{s}}_i - \mathbf{s}_0$ and

$$\mathbf{h}_i = \left[\frac{\partial \tilde{t}_i}{\partial \mathbf{s}_i}\right]^T_{\mathbf{s}_i=\tilde{\mathbf{s}}_i} = \frac{1}{c}\frac{\tilde{\mathbf{s}}_{i0}}{\sqrt{\tilde{\mathbf{s}}_{i0}^T\tilde{\mathbf{s}}_{i0}}} \tag{17}$$

The total TOA measurement error is:

$$\delta t_i = \mathbf{h}_i^T \delta \mathbf{s}_i + v_i \tag{18}$$

and the TOA covariance is:

$$R_t = \mathrm{cov}\left\{\delta t_i\right\} = \mathbf{h}_i^T R_s \mathbf{h}_i + \sigma_t^2 \tag{19}$$

The cluster TDOAs are combined to a Range-Differences (RDs) vector:

$$\tilde{\mathbf{r}} = c\left[\tilde{t}_2 - \tilde{t}_1, \tilde{t}_3 - \tilde{t}_1, \ldots, \tilde{t}_N - \tilde{t}_1\right]^T \tag{20}$$

and the RDs covariance $R = \mathrm{cov}\left\{\tilde{\mathbf{r}}\right\}$ is:

$$\begin{aligned} R &= c^2 \mathbf{h}_1^T R_s \mathbf{h}_1 \cdot \underline{1}_{d_r}\underline{1}_{d_r}^T + \\ &+c^2 \begin{bmatrix} \mathbf{h}_2^T \\ \vdots \\ \mathbf{h}_N^T \end{bmatrix} R_s \begin{bmatrix} \mathbf{h}_2 & \cdots & \mathbf{h}_N \end{bmatrix} + \\ &+c^2\sigma_t^2 \cdot \left[I_{d_r\times d_r} + \underline{1}_{d_r}\underline{1}_{d_r}^T\right] \end{aligned} \tag{21}$$

where $d_r = N - 1$ and

$$\underline{1}_{d_r}^T \triangleq \begin{bmatrix} 1 & 1 & \cdots & 1 \end{bmatrix}_{1\times d_r}. \tag{22}$$

2.3.2 RDs Fisher Information Matrix

For unbiased measurements with additive Gaussian noise the Fisher Information Matrix (FIM) is:

$$J\left(\boldsymbol{\theta}\right) = H\left(\boldsymbol{\theta}\right)^T R^{-1} H\left(\boldsymbol{\theta}\right) + \frac{1}{2}\Delta\left(\boldsymbol{\theta}\right) \tag{23}$$

where $\boldsymbol{\theta}$ is the unknown parameter vector , R is the measurement error covariance and $\Delta\left(\boldsymbol{\theta}\right)$ is (with index summation convention):

$$\left[\Delta\left(\boldsymbol{\theta}\right)\right]_{mn} = \left[R^{-1}\right]_{ab}\frac{\partial R_{bc}}{\partial\theta_m}\left[R^{-1}\right]_{cd}\frac{\partial R_{da}}{\partial\theta_n} \tag{24}$$

$$\left\{\begin{array}{c} a,b,c,d = 1,2,\ldots,N-1 \\ m,n = 1,2,3 \end{array}\right\}$$

For the RD measurements R is given in Eq.(21) and:

$$H\left(\boldsymbol{\theta}\right) = \left.\frac{\partial\tilde{\mathbf{r}}}{\partial\mathbf{s}_0}\right|_{\mathbf{s}_0=\boldsymbol{\theta}} = \left[\begin{array}{c} \mathbf{h}_1^T - \mathbf{h}_2^T \\ \vdots \\ \mathbf{h}_1^T - \mathbf{h}_N^T \end{array}\right]_{\mathbf{s}_0=\boldsymbol{\theta}} \tag{25}$$

3 Initialization Methods

An ideal RD measurement

$$r_{ij} = \left\|\mathbf{s}_{i0}\right\| - \left\|\mathbf{s}_{j0}\right\|, \tag{26}$$

is a compact form of the hyperboloid quadric:

$$\left(\mathbf{s}_0 - \mathbf{c}_{ij}\right)^T Q\left(\mathbf{s}_0 - \mathbf{c}_{ij}\right) = 1 \tag{27}$$

with foci at $\mathbf{s}_i$ and $\mathbf{s}_j$, where $\mathbf{c}_{ij} \triangleq \frac{\mathbf{s}_i+\mathbf{s}_j}{2}$ and the metric Q is

$$Q \triangleq \left(\frac{\mathbf{s}_{ij}^T\mathbf{s}_{ij} - r_{ij}^2}{4}\right)^{-1}\left[\frac{\mathbf{s}_{ij}\mathbf{s}_{ij}^T}{r_{ij}^2} - I\right]. \tag{28}$$

Applying the reverse triangle inequality on Eq. (26) we get $|r_{ij}| \leq \left\|\mathbf{s}_{ij}\right\|$, therefore the signature of Q is $(-,-,+)$ and it represents a two-sheet hyperboloid of revolution about $\mathbf{s}_{ij}$. Given three RDs, a hyperbolic fix of the beacon $\mathbf{s}_0$ is one of the intersection points of the three RD hyperboloids. In geolocation problems the beacon is known to be on the surface of Earth, therefore, the position could be obtained with two RDs from the intersection of the two RD hyperboloids and Earth's surface, as shown in Fig.1.

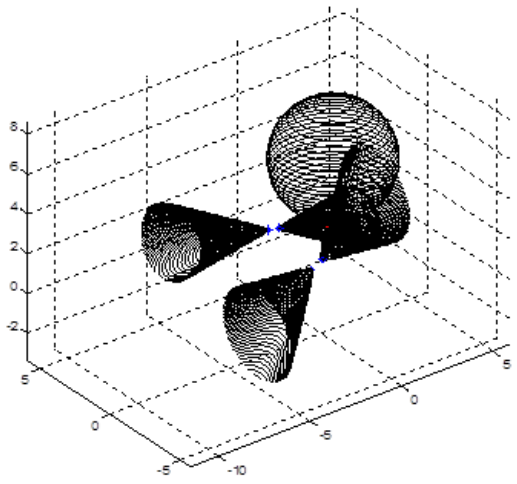

Figure 1: The intersection of two hyperboloids and a sphere

3.1 Initialization with three satellites

3.1.1 Ho and Chan's method

A formation of three satellites, including a leader $\mathbf{s}_1$, and two followers $\mathbf{s}_2$ and $\mathbf{s}_3$, produces two RDs from a single pulse:

$$\begin{aligned} r_{21} &= \|\mathbf{s}_{20}\| - \|\mathbf{s}_{10}\| \\ r_{31} &= \|\mathbf{s}_{30}\| - \|\mathbf{s}_{10}\| \end{aligned} \tag{29}$$

An exact solution has been presented by Ho and Chan[5], assuming a spherical Earth, where the beacon coordinates are a function of a single unknown parameter $r_1 \triangleq \|\mathbf{s}_{10}\|$:

$$\mathbf{s}_0 = A^{-1}\mathbf{b}\left(r_1\right) \tag{30}$$

where

$$A = -2\left[\begin{array}{ccc} \mathbf{s}_1 & \mathbf{s}_{21} & \mathbf{s}_{31} \end{array}\right]^T \tag{31}$$

and the vector $\mathbf{b}$ is a function of the unknown parameter r_1:

$$\mathbf{b} = \mathbf{b}_2 r_1^2 + \mathbf{b}_1 r_1 + \mathbf{b}_0 \tag{32}$$

with

$$\begin{aligned} \mathbf{b}_2 &= \left[\begin{array}{ccc} 1 & 0 & 0 \end{array}\right]^T \\ \mathbf{b}_1 &= \left[\begin{array}{ccc} 0 & 2r_{21} & 2r_{31} \end{array}\right]^T \\ \mathbf{b}_0 &= \left[\begin{array}{c} -r_\oplus^2 - \mathbf{s}_1^T\mathbf{s}_1 \\ r_{21}^2 - \left(2\mathbf{s}_1 + \mathbf{s}_{21}\right)^T\mathbf{s}_{21} \\ r_{31}^2 - \left(2\mathbf{s}_1 + \mathbf{s}_{31}\right)^T\mathbf{s}_{31} \end{array}\right] \end{aligned} \tag{33}$$

The solution for r_1 is obtained from applying the sphere constraint $\mathbf{s}_0^T\mathbf{s}_0 = r_\oplus^2$, where $r_\oplus$ is the equatorial Earth radius:

$$\mathbf{b}^T A^{-T} A^{-1}\mathbf{b} = r_\oplus^2 \tag{34}$$

which is a quartic of r_1:

$$\begin{aligned} f\left(r_1\right) &= \mathbf{b}^T W_A \mathbf{b} - r_\oplus^2 \\ &= k_4 r_1^4 + k_3 r_1^3 + k_2 r_1^2 + k_1 r_1 + k_0 \end{aligned} \tag{35}$$

where $W_A = A^{-T}A^{-1}$ and the quartic coefficients are:

$$\begin{aligned} k_4 &= \mathbf{b}_2^T W_A \mathbf{b}_2 \\ k_3 &= 2\mathbf{b}_2^T W_A \mathbf{b}_1 \\ k_2 &= 2\mathbf{b}_2^T W_A \mathbf{b}_0 + \mathbf{b}_1^T W_A \mathbf{b}_1 \\ k_1 &= 2\mathbf{b}_1^T W_A \mathbf{b}_0 \\ k_0 &= \mathbf{b}_0^T W_A \mathbf{b}_0 - r_\oplus^2 \end{aligned} \tag{36}$$

A solution could be obtained provided that A is full rank, applying the following conditions on the formation geometry:

$$\mathbf{s}_{21} \nparallel \mathbf{s}_{31} \quad , \quad \mathbf{s}_{21} \nparallel \mathbf{s}_1 \quad , \quad \mathbf{s}_{31} \nparallel \mathbf{s}_1 \tag{37}$$

3.1.2 Initial Ambiguity

The quartic $f\left(r_1\right)$ has up to four real positive roots. For a satellite formation $\|\mathbf{s}_1\| > \|\mathbf{s}_0\|$, therefore $r_1 \in [r_{min}, r_{max}]$. $r_{min} = \|\mathbf{s}_1\| - r_\oplus$ is the local altitude of $\mathbf{s}_1$ above the sphere and $r_{max} = \sqrt{\|\mathbf{s}_1\|^2 - r_\oplus^2}$ is the distance to the local horizon of $\mathbf{s}_1$. When two or more solutions are in the range $[r_{min}, r_{max}]$ there is an ambiguity in the initial beacon position. The condition for this depends on the cluster geometry with respect to the beacon. Each of the N_0 roots $\left\{r_1^{(i)}\right\}_{i=1}^{N_0} \in [r_{min}, r_{max}]$ corresponds to different positions: $\hat{\mathbf{s}}_0^{(i)}$, an estimate of the true beacon position or a phantom. These positions are equivalent in the sense of the measurements, i.e., if the pulse was transmitted from either positions, the same TDOAs would have been measured in the formation. Only additional information could resolve this ambiguity.

3.1.3 Non-Spherical Earth model

The spherical constraint is a zero order Earth surface model with an error in the local radius increasing with the latitude up to about 20km at the poles. A more accurate model is the oblate sphere ellipsoid:

$$\mathbf{s}_0^T P_\oplus^{-1}\mathbf{s}_0 = r_\oplus^2 \tag{38}$$

where $P_\oplus$ is

$$P_\oplus = \left[\begin{array}{ccc} 1 & 0 & 0 \\ 0 & 1 & 0 \\ 0 & 0 & \left(1 - f_\oplus\right)^2 \end{array}\right] \tag{39}$$

and $f_\oplus$ is the flattening factor. With the ellipsoid constraint the exact solution in Eq.(30) could not be applied directly and the following iterative method is applied:

1. The ellipsoid constrain is replaced with a sphere constrain:

$$\left(\hat{\mathbf{s}}_{0(k)}^{(i)}\right)^T \hat{\mathbf{s}}_{0(k)}^{(i)} = \left(\hat{r}_{L(k)}^{(i)}\right)^2 \tag{40}$$

where $\hat{r}_{L(k)}^{(i)}$ is an estimate (after k iterations) of $r_L^{(i)}$, the local Earth radius at the position of $\mathbf{s}_{0(k)}^{(i)}$. $\hat{r}_L^{(i)}$ is initialized with the leader's local Earth radius:

$$\hat{r}_{L(0)}^{(i)} = \sqrt{\frac{\mathbf{s}_1^T\mathbf{s}_1}{\mathbf{s}_1^T P_\oplus^{-1}\mathbf{s}_1}}\, r_\oplus \tag{41}$$

2. By replacing $r_\oplus$ with $\hat{r}^{(i)}_{L(k)}$, the exact method provides an estimate of $\hat{\mathbf{s}}^{(i)}_{0(k)}$. The local radius estimate is then updated for each of the N_0 initial estimates:

$$\hat{r}^{(i)}_{L(k+1)} = \sqrt{\frac{\left(\hat{\mathbf{s}}^{(i)}_{0(k)}\right)^T \hat{\mathbf{s}}^{(i)}_{0(k)}}{\left(\hat{\mathbf{s}}^{(i)}_{0(k)}\right)^T P_\oplus^{-1} \hat{\mathbf{s}}^{(i)}_{0(k)}}} r_\oplus \tag{42}$$

3. The iterations continue until convergence of $\hat{r}^{(i)}_{L(k)}$.

3.2 Initialization with two satellites

For a formation of two satellites, a leader $\mathbf{s}_1$, and a follower $\mathbf{s}_2$, the two necessary RDs could only be obtained from two pulses:

$$\begin{aligned} r_{21} &= \|\mathbf{s}_{20}\| - \|\mathbf{s}_{10}\| \\ r_{43} &= \|\mathbf{s}_{40}\| - \|\mathbf{s}_{30}\| \end{aligned} \tag{43}$$

where $\mathbf{s}_3$ and $\mathbf{s}_4$ are the positions of the leader and follower $\mathbf{s}_1$ and $\mathbf{s}_2$ at the TOA of the second pulse. The exact solution in Eq.(30) does not apply directly in this case, however we suggest the following modification:

$$\mathbf{s}_0 = A^{-1}\mathbf{b}\left(r_1, r_3\right) \tag{44}$$

where $r_3 \triangleq \|\mathbf{s}_{30}\|$ and

$$A = -2\left[\begin{array}{ccc} \mathbf{s}_1 & \mathbf{s}_{21} & \mathbf{s}_{43} \end{array}\right]^T \tag{45}$$

By introducing the scalar $a > 0$:

$$a \triangleq \frac{r_3}{r_1} \tag{46}$$

we can present the vector $\mathbf{b}\left(r_1, r_3\right)$ as a function of r_1 and a:

$$\mathbf{b}\left(r_1, a\right) = \mathbf{b}_2 r_1^2 + \mathbf{b}_1\left(a\right) r_1 + \mathbf{b}_0 \tag{47}$$

with:

$$\begin{aligned} \mathbf{b}_2 &= \left[\begin{array}{ccc} 1 & 0 & 0 \end{array}\right]^T \\ \mathbf{b}_1 &= \left[\begin{array}{ccc} 0 & 2r_{21} & 2r_{43}\cdot a \end{array}\right]^T \\ \mathbf{b}_0 &= \left[\begin{array}{c} -r_\oplus^2 - \mathbf{s}_1^T\mathbf{s}_1 \\ r_{21}^2 - \left(2\mathbf{s}_1 + \mathbf{s}_{21}\right)^T \mathbf{s}_{21} \\ r_{31}^2 - \left(2\mathbf{s}_3 + \mathbf{s}_{43}\right)^T \mathbf{s}_{43} \end{array}\right] \end{aligned} \tag{48}$$

The quartic $f\left(r_1, a\right) = 0$ coefficients are as in Eq.(36) with the modified $\mathbf{b}\left(r_1, a\right)$ vector components in Eq.48. The following iterative method is then applied:

1. For a given $a_{(k)}$ we solve the quartic $f\left(r_1, a_{(k)}\right) = 0$ and obtain $\left\{\mathbf{s}^{(i)}_{0(k)}\right\}_{i=1}^{N_0}$. In the case that the two pulses are transmitted in an interval $\Delta T \ll \frac{\|\mathbf{s}_{21}\|}{\|\dot{\mathbf{s}}_1\|}$ we get $r_1 \approx r_3$, therefore we choose $a_{(0)} = 1$ to initialize the algorithm.

2. A consistent choice of $\mathbf{s}^{(i)}_{0(k)}$ is then used to obtain $a_{(k+1)}$ for the next iteration:

$$a_{(k+1)} = \frac{\left\|\mathbf{s}_3 - \mathbf{s}^{(i)}_{0(k)}\right\|}{r_1\left(a_{(k)}\right)} \tag{49}$$

3. The iterations are performed until the convergence of a.

4. If the ellipsoid constraint in Eq.(38) is used, combined iterations are performed for a and r_L.

This combined iteration method provides the intersection points of two hyperboloids of revolution and an oblate sphere and has been shown to converge in simulations. A convergence analysis is subject for additional studies, based on the fact that both a and r_L are bounded. $\mathbf{s}_0$ is in the horizon of both $\mathbf{s}_1$ and $\mathbf{s}_3$, therefore a is bounded in the range:

$$a \in \left[\frac{\|\mathbf{s}_3\| - r_\oplus}{\sqrt{\|\mathbf{s}_1\|^2 - r_\oplus^2}}, \frac{\sqrt{\|\mathbf{s}_3\|^2 - r_\oplus^2}}{\|\mathbf{s}_1\| - r_\oplus}\right] \tag{50}$$

and r_L is bounded between the polar and equatorial radii :

$$r_L \in \left[\left(1 - f_\oplus\right), 1\right] \cdot r_\oplus \tag{51}$$

Initializing with two satellites and two measurements does not solve the ambiguity problem as will be shown in the following results.

3.3 Initial Estimate covariance

The covariance of $\hat{\mathbf{s}}^{(i)}_0$ is:

$$P^{(i)}_0 = \tilde{H}^{-1} R_0\left(\hat{\mathbf{s}}^{(i)}_0\right) \tilde{H}^{-T} \tag{52}$$

where

$$\tilde{H} = \left[\begin{array}{c} H\left(\hat{\mathbf{s}}^{(i)}_0\right) \\ 2\left(\hat{\mathbf{s}}^{(i)}_0\right)^T P_\oplus^{-1} \end{array}\right] \tag{53}$$

3.3.1 Initial estimate covariance for three satellites

$$H(\mathbf{s}_0) = \begin{bmatrix} \mathbf{h}_1^T - \mathbf{h}_2^T \\ \mathbf{h}_1^T - \mathbf{h}_3^T \end{bmatrix} \quad (54)$$
$$R_0 = \begin{bmatrix} R & 0_{2\times 1} \\ 0_{1\times 2} & 0 \end{bmatrix}$$

where R is the RDs covariance as in Eq.21 for $N = 3$.

3.3.2 Initial estimate covariance for two satellites

$$H(\mathbf{s}_0) = \begin{bmatrix} \mathbf{h}_1^T - \mathbf{h}_2^T \\ \mathbf{h}_3^T - \mathbf{h}_4^T \end{bmatrix} \quad (55)$$
$$R_0 = \begin{bmatrix} R_{21} & 0 & 0 \\ 0 & R_{43} & 0 \\ 0 & 0 & 0 \end{bmatrix}$$

where

$$R_{ij} = c^2 \mathbf{h}_i^T R_s \mathbf{h}_i + c^2 \mathbf{h}_j^T R_s \mathbf{h}_j + 2 \cdot c^2 \sigma_t^2 \quad (56)$$

4 Filtering Method

4.1 SMM-EKF with TDOA measurements

In the case that additional pulses are measured, the initial ambiguity could be resolved. For a sequential estimator we choose to apply a Static Multiple Model (SMM) scheme [10] with N_0 hypothesis corresponding to the initial estimates $\left\{\hat{\mathbf{s}}_0^{(i)}\right\}_{i=1}^{N_0}$ and covariances $\left\{P_0^{(i)}\right\}_{i=1}^{N_0}$:

$$\mathcal{M}_i = \left\{\hat{\mathbf{s}}_0^{(i)}(t_0), P_0^{(i)}(t_0), F_k^i, B_k^i, G_k^i, R_k^i, Q_k^i\right\} \quad (57)$$

The initial mode matched probabilities $\{\mu_i\}_{i=1}^{N_0}$ are chosen to reflect the equivalence of the phantom and the true target:

$$\mu_i = \frac{1}{N_0} \quad (58)$$

For each mode an extended Kalman filter (EKF) estimator is used with:

$$F_k^i = I \quad , \qquad B_k^i = G_k^i = Q_k^i = 0 \quad (59)$$

H_k^i and R_k^i are calculated according to Eq. (25) and Eq. (21) with $\mathbf{s}_0 = \hat{\mathbf{s}}_0^{(i)}$. The SMM algorithm flow chart for resolving initial ambiguity is shown in Fig.2 .

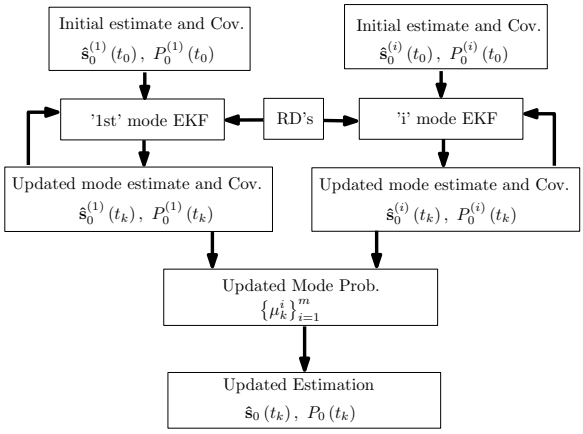

Figure 2: SMM flow chart

4.2 Estimation Bounds

The FIM of the sequence of RDs is:

$$I_M = \sum_{k=1}^{M} J_k \quad (60)$$

where J_k is calculated according to Eq.(23). The Cramer-Rao lower bound (CRLB) is:

$$E\left[(\hat{\mathbf{s}}_0 - \mathbf{s}_0)^T (\hat{\mathbf{s}}_0 - \mathbf{s}_0)\right] \geq \mathrm{tr}\left\{I_M^{-1}\right\} \quad (61)$$

For the CRLB to be calculated I_M must be full rank and it does not incorporate constrains. In this study the target is constrained to the earth surface, and the initial FIM is singular, therefore, a constrained CRLB is the correct lower bound[11]:

$$E\left[(\hat{\mathbf{s}}_0 - \mathbf{s}_0)^T (\hat{\mathbf{s}}_0 - \mathbf{s}_0)\right] \geq \mathrm{tr}\left\{\mathcal{U}\left[\mathcal{U}^T I_M \mathcal{U}\right]^\dagger \mathcal{U}^T\right\} \quad (62)$$

where $[]^\dagger$ denotes the Moore–Penrose pseudo-inverse and $\mathcal{U}(\mathbf{s}_0)$ is an orthonormal basis of the null space of $\mathcal{R}(\mathbf{s}_0)$, the normal space to the constrain at $\mathbf{s}_0$:

$$\mathcal{R}(\mathbf{s}_0)\mathcal{U}(\mathbf{s}_0) = \mathbf{0} \quad , \qquad \mathcal{U}^T\mathcal{U} = I \quad (63)$$

For the oblate sphere model the constrain is:

$$r(\mathbf{s}_0) = \mathbf{s}_0^T P_\oplus^{-1} \mathbf{s}_0 - r_\oplus^2 = 0 \quad (64)$$

therefore,

$$\mathcal{R}(\mathbf{s}_0) = \frac{\partial r(\mathbf{s}_0)}{\partial \mathbf{s}_0} = \mathbf{s}_0^T P_\oplus^{-1} \quad (65)$$

$\mathcal{U} = \begin{bmatrix} \hat{\mathbf{u}}_1 & \hat{\mathbf{u}}_2 \end{bmatrix}$ could be chosen to be the East-North subspace of the local East-North-Up (ENU)

frame where $\hat{\mathbf{u}}_1 = -[\hat{\mathbf{n}}\times]\,\hat{\mathbf{z}}$, $\hat{\mathbf{u}}_2 = -[\hat{\mathbf{n}}\times]^2\,\hat{\mathbf{z}}$ and where $\hat{\mathbf{n}}(\mathbf{s}_0)$ is the local normal unit vector:

$$\hat{\mathbf{n}}(\mathbf{s}_0) = \frac{P_{\oplus}^{-1}\mathbf{s}_0}{\sqrt{\mathbf{s}_0^T P_{\oplus}^{-2}\mathbf{s}_0}} \tag{66}$$

The transformation from the ECEF frame $\mathcal{F}$ to the local ENU frame $\mathcal{L}$ is then $\mathcal{T}_{\mathcal{F}2\mathcal{L}} = \left[\begin{array}{cc} \mathcal{U} & \hat{\mathbf{n}} \end{array}\right]^T$.

5 Results

5.1 Setup

A three-satellite cluster is propagated along Keplerian orbits starting from the initial orbital elements:

$$\begin{aligned} \mathbf{e}_1 &= \{a_1, e_1, i_1, \omega_1, \Omega_1, \nu_1, M_1\} \\ \mathbf{e}_2 &= \{a_1, e_1, i_1, \omega_1, \Omega_1 + \varepsilon_2, \nu_1 + \phi_2, M_1\} \\ \mathbf{e}_3 &= \{a_1, e_1, i_1, \omega_1, \Omega_1 + \varepsilon_3, \nu_1 + \phi_3, M_1\} \end{aligned} \tag{67}$$

We examine a quasi-planar satellite formation where the leader $\mathbf{s}_1$ is on a circular orbit ($e_1 = 0$), while $\mathbf{s}_2$ and $\mathbf{s}_3$ are phased from $\mathbf{s}_1$ by small anomaly angles ϕ_2, $\phi_3 \ll 1$ and perturbed out of the plane by RAAN differences ε_2, $\varepsilon_3 \ll 1$. A quasi-planar formation is an extremely poor geometry for geolocation, however it is beneficial for long term formation keeping[12] and hence the case study for this work. The distance between the satellites is chosen to be approximately $\|\mathbf{s}_{21}\| = \|\mathbf{s}_{32}\| \approx 100$km, from which we determine ϕ_2 and $\phi_3 = 2 \cdot \phi_2$:

$$\phi_2 = -2 \cdot \sin^{-1}\left(\frac{\|\mathbf{s}_{21}\|}{2 \cdot a_1}\right) \tag{68}$$

All perturbing dynamics [13] are neglected along the examined 100 seconds. A beacon is positioned on Earth's surface in the horizon of the initial position of $\mathbf{s}_1$. The surface model used is the WGS-84 ellipsoid. The beacon transmits 10 consecutive pulses with a pulse repetition interval of $\Delta T = 10$sec. The Earth's spin vector is assumed constant during the examined 100 sec:

$$\mathbf{\Omega}_{\oplus} = [0, 0, \Omega_{\oplus}]^T \tag{69}$$

The covariance of the satellite position estimate is modeled as:

$$R_s = \sigma_s^2 \cdot I_{3\times 3} \tag{70}$$

All formation simulation parameters are given in Table 1.

Table 1: Setup Values

Symbol	Value	Units
$\Omega_{\oplus}$	$7.292 \cdot 10^5$	$\frac{rad}{sec}$
$\mu_{\oplus}$	$3.986 \cdot 10^5$	$\frac{km^3}{sec^2}$
$r_{\oplus}$	6378.198	km
Ω_1	0	deg
ω_1	0	deg
i_1	50	deg
a_1	7078.1	km
e_1	0	
M_1	0	deg
ε_2	-0.0278	deg
ε_3	0	deg

5.2 CRLB Map

In order to obtain some insight about the predicted performance of the method CRLB maps are created according to Eq.(62) and shown in Fig.3 and Fig.4. The map levels represent the constrained CRLB values (in km) for a sequence of 10 pulses for different beacon positions on the constraint, with the same formation trajectories. These CRLB values are the best positioning performance we can obtain, in a root mean-squares (RMS) sense, with the given formation trajectories and measurement noise levels. For each case we examine two maps, one for low measurement noise levels ($\sigma_t = 20$nsec) and the other for high noise levels ($\sigma_t = 100$nsec). For both cases the the navigation $1-\sigma$ error is $\sigma_s = 5$m. The red marks in the map represent the initial and final positions of the leader, $\mathbf{s}_1$, projected onto the constraint. We notice that the CRLB deteriorates significantly along the formation ground track and that the best conditions are achieved perpendicular to the ground track. The three satellite formation provides a lower bound than the two satellite formation with twice the number of measurements.

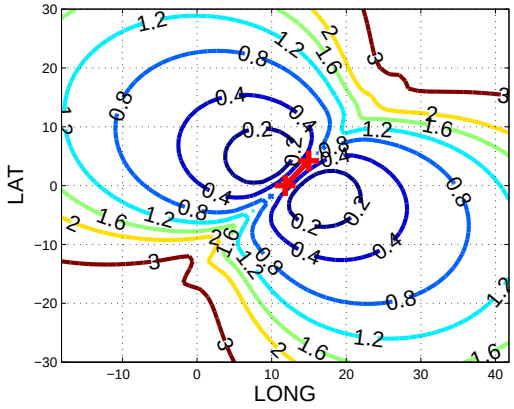

(a) CRLB map for $\sigma_s = 5$m, $\sigma_t = 20$nsec

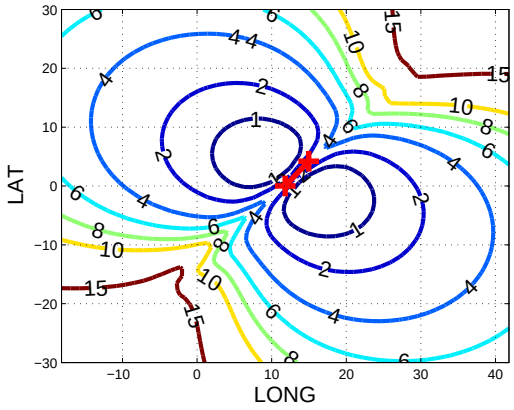

(b) CRLB map for $\sigma_s = 5$m, $\sigma_t = 100$nsec

Figure 3: Three Satellite Formation Constrained CRLB Map

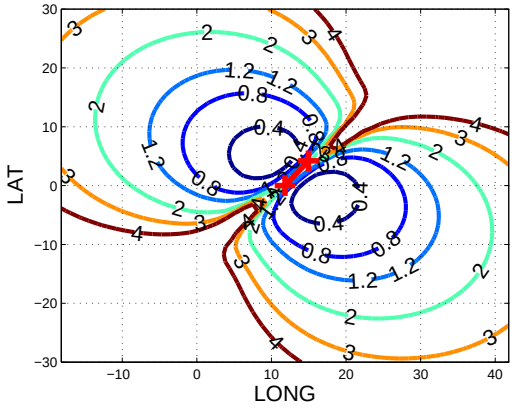

(a) CRLB map for $\sigma_s = 5$m, $\sigma_t = 20$nsec

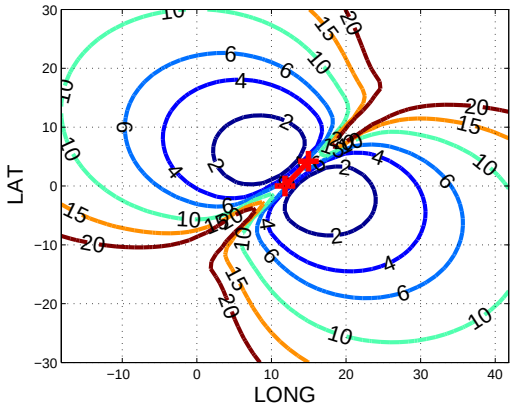

(b) CRLB map for $\sigma_s = 5$m, $\sigma_t = 100$nsec

Figure 4: Two Satellite Formation Constrained CRLB Map

5.3 Case study

We examine a beacon positioned in an intermediate initial range $r_1 = 1477$km, where $r_{max} \approx 3070$km and $r_{min} \approx 700$km. The scenario is examined twice, first with the three satellite formation, and second with only two of the three satellites, $\mathbf{s}_1$ and $\mathbf{s}_2$ taken from the same three satellite positions sequence. For both cases there is an initial ambiguity, as shown in Fig. 5.

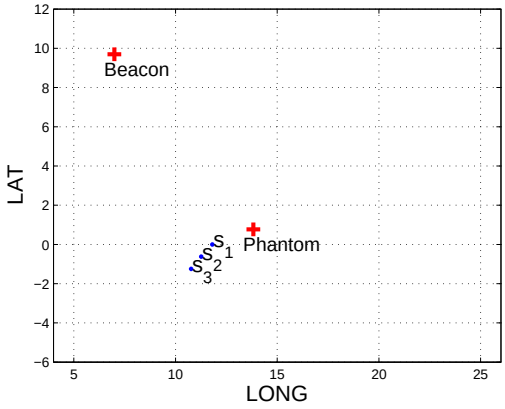

(a) Initialization with three satellites

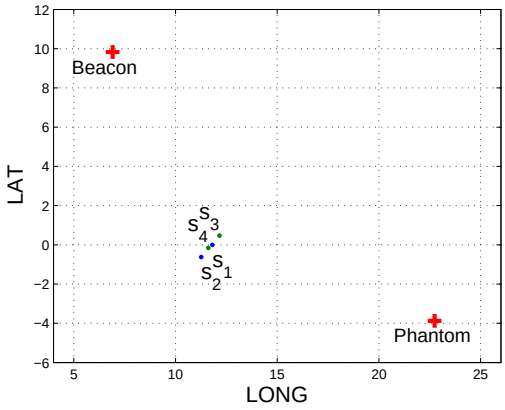

(b) Initialization with two satellites

Figure 5: Quasi-planar formation and target ambiguity

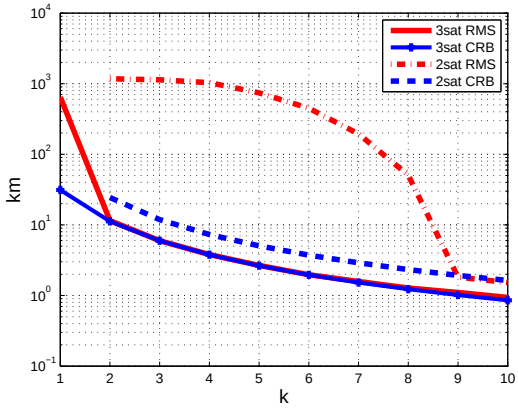

(a) Estimation RMS and CRLB

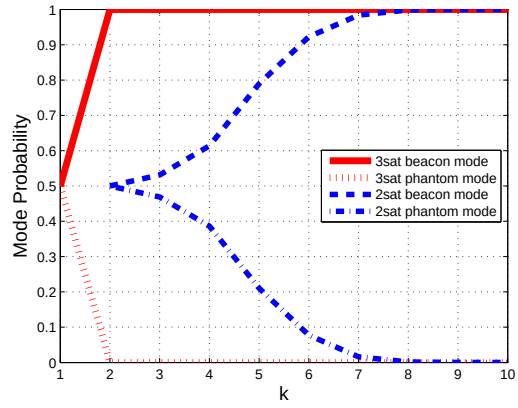

(b) SMM mode probabilities

Figure 6: SMM Monte Carlo Results

RMS results and averaged mode probabilities are calculated for based on 1000 Monte Carlo runs for the high noise levels case with $\sigma_s = 5$m and $\sigma_t = 100$nsec. As shown in Fig.6, the SMM processing the measurements of the three satellite formation (two RDs per pulse) achieves the constrained CRLB and identifies the true target with two pulses, where the two satellite SMM (one RD per pulse) identifies the true target after 7 pulses (with a 0.99 probability) and achieves the CRLB after 9 pulses. The initial RMS error is hundreds of km because the SMM takes the midpoint between the true target and the phantom as the initial estimate. The final RMS error is 1km and 2km for the two and three satellite formations.

6 Conclusions

We presented an initialization method with a two satellite formation and have demonstrated the usefulness of a SMM scheme in solving the initial ambiguity. A Constrained CRLB map has been contracted for the problem and Monte Carlo runs have shown the efficiency of the method for the examined case. The proposed method can be implemented in real-time geolocation applications for two and three satellite formations.

References

[1] Foy, W., "Position-location solutions by Taylor-series estimation," *IEEE Transactions on Aerospace and Electronic Systems*, , No. 2, 1976, pp. 187–194.

[2] Friedlander, B., "A passive localization algorithm and its accuracy analysis," *IEEE Journal of Oceanic Engineering*, Vol. 12, No. 1, 1987, pp. 234–245.

[3] Smith, J. and Abel, J., "Closed-form least-squares source location estimation from range-difference measurements," *IEEE Transactions on Acoustics, Speech and Signal Processing*, Vol. 35, No. 12, 1987, pp. 1661–1669.

[4] Li, L. and Wei, F., "Position Estimation by Improved Genetic Algorithm for Hyperbolic Location," *14th IST Mobile & Wireless Communications*, 2005.

[5] Ho, K. and Chan, Y., "Geolocation of a known altitude object from TDOA and FDOA measurements," *IEEE Transactions on Aerospace and Electronic Systems*, Vol. 33, No. 3, 1997, pp. 770–783.

[6] Okello, N., Fletcher, F., Musicki, D., and Ristic, B., "Comparison of Recursive Algorithms for Emitter Localisation using TDOA Measurements from a Pair of UAVs," *IEEE Transactions on Aerospace and Electronic Systems*, Vol. 47, No. 3, 2011, pp. 1723–1732.

[7] Savage, C., Cramer, R., and Schmitt, H., "TDOA geolocation with the unscented Kalman filter," *IEEE International Conference on Networking, Sensing and Control*, 2006, pp. 602–606.

[8] Fletcher, F., Ristic, B., and Musicki, D., "Recursive estimation of emitter location using TDOA measurements from two UAVs," *10th International Conference on Information Fusion*, IEEE, 2007, pp. 1–8.

[9] Musicki, D., Kaune, R., and Koch, W., "Mobile emitter geolocation and tracking using TDOA and FDOA measurements," *IEEE Transactions on Signal Processing*, Vol. 58, No. 3, 2010, pp. 1863–1874.

[10] Bar-Shalom, Y., Li, X.-R., and Kirubarajan, T., *Estimation with Applications to Tracking and Navigation*, John Wiley & Sons, Inc., 2002, pp. 441–443.

[11] Ben-Haim, Z. and Eldar, Y., "On the constrained Cramér–Rao bound with a singular Fisher information matrix," *Signal Processing Letters, IEEE*, 2009.

[12] Gurfil, P., Herscovitz, J., and Pariente, M., "The SAMSON Project - Cluster Flight and Geolocation with Three Autonomous Nanosatellites," *26th AIAA/USU Conference on Small Satellites*, Salt Lake City, UT, USA, August 2012.

[13] Alfriend, K., Vadali, S., Gurfil, P., How, J., and Breger, L., *Spacecraft formation flying: dynamics, control, and navigation*, Elsevier, 2010.